Reconstructing Compressor Non-Uniform Circumferential Flow Field From Spatially Undersampled Data—Part 1: Methodology and Sensitivity Analysis

Fangyuan Lou[1]
School of Mechanical Engineering,
Purdue University,
West Lafayette, IN 47907
e-mail: louf@purdue.edu

Nicole L. Key
School of Mechanical Engineering,
Purdue University,
West Lafayette, IN 47907
e-mail: nkey@purdue.edu

The flow field in a compressor is circumferentially non-uniform due to the wakes from upstream stators, the potential field from both upstream and downstream stators, and blade row interactions. This non-uniform flow impacts stage performance as well as blade forced vibrations. Historically, experimental characterization of the circumferential flow variation is achieved by circumferentially traversing either a probe or the stator rows. This involves the design of complex traverse mechanisms and can be costly. To address this challenge, a novel method is proposed to reconstruct compressor non-uniform circumferential flow field using spatially under-sampled data points from a few probes at fixed circumferential locations. The paper is organized into two parts. In the present part of the paper, details of the multi-wavelet approximation for the reconstruction of circumferential flow and use of the particle swarm optimization algorithm for selection of probe positions are presented. Validation of the method is performed using the total pressure field in a multi-stage compressor representative of small core compressors in aero engines. The circumferential total pressure field is reconstructed from eight spatially distributed data points using a triple-wavelet approximation method. Results show good agreement between the reconstructed and the true total pressure fields. Also, a sensitivity analysis of the method is conducted to investigate the influence of probe spacing on the errors in the reconstructed signal. [DOI: 10.1115/1.4050433]

Keywords: flow reconstruction, spatially under-sampled data, compressor non-uniform circumferential flow, multi-wavelet approximation, particle swarm optimization, measurement techniques

Introduction

The flow field in a compressor is circumferentially non-uniform. The circumferential variations measured in the absolute reference frame are associated with the wakes from upstream stator row(s), potential fields from both upstream and downstream stator rows, and their aerodynamic interactions. Also, stator–stator and rotor–rotor interactions can impact stage performance. For example, the numerical study conducted by He et al. [1] in a 2.5-stage transonic axial compressor showed a 0.1% efficiency variation due to stator–stator interactions and a maximum of 0.7% variation in efficiency caused by rotor–rotor interactions. The effect of stator–stator interactions on stage performance has been investigated using vane clocking, the circumferential indexing of adjacent vane rows with the same vane count. For example, the study conducted by Key et al. [2] in a three-stage axial compressor showed a 0.27-point variation in the isentropic efficiency of the embedded stage at the design loading condition and a 1.07-point variation in the embedded stage efficiency at a high loading condition with changes in vane clocking configurations. The experimental characterization of stage efficiency is facilitated when similar vane counts exist because that means that measuring the flow across a single vane passage will accurately capture the full-annulus performance. This is great for research, but it is not a common luxury for real compressors, in which the stators typically have different vane counts requiring measurements over several pitches, if not the entire annulus, to accurately capture the circumferential flow variations.

Blade row interactions can also affect rotor resonant response. The resonant response of a rotor blisk is driven by the forcing functions, aero-damping, and mistuning. The forcing function for rotor resonant response consists of wakes from upstream stator rows, the potential field of both upstream and downstream stator rows, and their aerodynamic interactions. In the study conducted by Choi et al. [3], results showed 80% differences in the mean blade response at design loading and 168% differences in the mean blade response at high loading by varying the clocking of the upstream stator rows. A follow-up computational study performed by Salontay et al. [4] showed that the variations in the blade response are caused by the changes in the phase between the rotor upstream vortical and downstream potential forcing functions.

In addition to the primary excitations including the wakes from upstream stator rows and the potential fields from the downstream vanes, acoustic modes (also known as Tyler–Sofrin modes) generated by rotor–stator interactions occur at blade passing frequency and can contribute to rotor resonance. In a recent two-part study conducted by Terstegen et al. [5] and Sanders et al. [6], the existence of the acoustic Tyler–Sofrin modes was confirmed experimentally in a three-stage axial compressor, and the corresponding

[1]Corresponding author.

Contributed by the International Gas Turbine Institute (IGTI) of ASME for publication in the Journal of Turbomachinery. Manuscript received November 12, 2020; final manuscript received January 25, 2021; published online April 26, 2021. Tech. Editor: David G. Bogard.

analysis demonstrated the importance of acoustic rotor–stator interactions for blade resonant response.

Additionally, the circumferentially non-uniform flow can introduce instrumentation errors in calculating compressor performance during rig or engine tests. To characterize the performance of a compressor, rakes are typically equally spaced at several stations (fixed axial positions) around the annulus [7]. At each station, the thermodynamic properties acquired from the probes at different locations are averaged to a single value to represent the mean flow property. Historically, a simple area-average has been used because of the associated simplicity in implementation. Other averaging methods have emerged including mass-average, work-average, and momentum-average methods [8] during the past few decades, all of which require additional flow field information. However, regardless of the different averaging methods used, without the detailed information of flow properties around the full annulus, the accuracy of the averaged value as a representation of the true mean flow property is limited, and understanding how much error it can introduce into the calculation of compressor performance is critical. To answer this question, Stummann et al. [9] conducted a full-annulus unsteady Reynolds-averaged Navier–Stokes (URANS) simulation in a 3.5-stage axial compressor at mid-span and showed that the circumferentially non-uniform flow can cause more than a one-point error in compressor stage performance measurements. In a recent study, Chilla et al. [10] investigated the instrumentation errors caused by circumferential flow variations in an eight-stage axial compressor representative small core compressor of an aero-engine. The analysis showed that a baseline probe configuration with three equally spaced probes around the annulus yields a maximum of 0.8% error in flow capacity and 2.8 points error in compressor isentropic efficiency. Since designers are working hard to find efficiency improvements on the order of 0.1 points, a 2.8-point uncertainty in efficiency is not sufficient for confirmation of typical performance improvements in technology development programs.

Therefore, it is of great value to resolve the compressor non-uniform circumferential flow for precise calculation of compressor performance, as well as better prediction of blade forced response. Historically, experimental characterization of the circumferential flow variation is achieved by circumferentially traversing the flow, either utilizing a probe traverse mechanism or utilizing fixed instrumentation while actuating the stator rows circumferentially. This involves the design of complex traverse mechanisms that are challenging to seal and can be costly. To the best of the authors knowledge, there is a dearth of research available in the open literature on reconstructing compressor circumferentially non-uniform flow using spatially under-sampled data from a few probes at fixed circumferential locations. This motivates the work presented in this paper.

Scope of the Paper. The scope of the present part of the paper is to establish a roadmap for reconstructing the compressor circumferentially non-uniform flow from spatially under-sampled data. Below are the steps taken to achieve this objective:

(1) Introduce a novel multi-wavelet approximation method for reconstructing the circumferential flow.
(2) Draw practical guidelines for selection of the most important wavenumbers.
(3) Establish the procedure for the selection of probe count and optimal probe positioning.
(4) Provide measures for evaluation of the confidence in the reconstructed flow.

The paper is organized in the following manner. First, details of the multi-wavelet approximation method for signal reconstruction, particle swarm optimization (PSO) for probe position optimization, and definitions of the Pearson correlation coefficient and fitting residuals to evaluate the confidence in the reconstructed signal are described in the methodology section. Then, the method validation is presented using a total pressure field in a multi-stage compressor available in the open literature. In the final part of the paper, a sensitivity analysis of the method is conducted to quantify the influence of probe positioning on the error in the reconstructed signal.

Methodology

In theory, the circumferential flow field in turbomachines with a spatial periodicity of 2π can be described in terms of infinite serial wavelets of different wavenumbers:

$$x(\theta) = c_0 + \sum_{i=1}^{\infty} (A_i \sin(W_{n,i}\theta + \varphi_i)) \tag{1}$$

in which, $x(\theta)$ represents the flow property along the circumferential direction, c_0 represents the DC component of the signal, $W_{n,i}$ represents the ith wavenumber, and A_i and φ_i represent the magnitude and phase of the wavelet of the ith wavenumber. Furthermore, defining $a_i = A_i \cos \varphi_i$ and $b_i = A_i \sin \varphi_i$, Eq. (1) can be cast as:

$$x(\theta) = c_0 + \sum_{i=1}^{\infty} (a_i \sin(W_{n,i}\theta) + b_i \cos(W_{n,i}\theta)) \tag{2}$$

Multi-Wavelet Approximation Method. Research shows that the circumferential flow in a multi-stage compressor is typically dominated by several wavenumbers. In the study performed by Chilla et al. [10] on the circumferential variations of the stagnation pressure and temperature flow field in an eight-stage axial compressor representative of an aero-engine core compressor, results showed that the dominant wavenumber in the front and middle of the compressor is the upstream stator vane count, and the dominant wavenumber in the rear of the compressor is associated with the struts in the exit duct. For example, Fig. 1 shows the circumferential total pressure field and associated dominant wavenumbers at mid-span upstream of stator 6 in the compressor studied by Chilla et al. [10]. The circumferential variations in the total pressure field are dominated by seven wavenumbers associated with the vane counts of the blade rows upstream and downstream of stator 6 (from engine section stator (ESS)/inlet guide vane (IGV) to S6).

Therefore, instead of using an infinite number of wavelets described in Eq. (1), the circumferential flow in the compressor can be approximated by a few (N) dominant wavelets:

$$x(\theta) \approx c_0 + \sum_{j=1}^{N} (a_j \sin(W_{n,j}\theta) + b_j \cos(W_{n,j}\theta)) \tag{3}$$

This is an important step toward reconstructing the circumferential flow field since it reduces the number of unknown coefficients from infinity in Eq. (1) to $2N+1$ in Eq. (2).

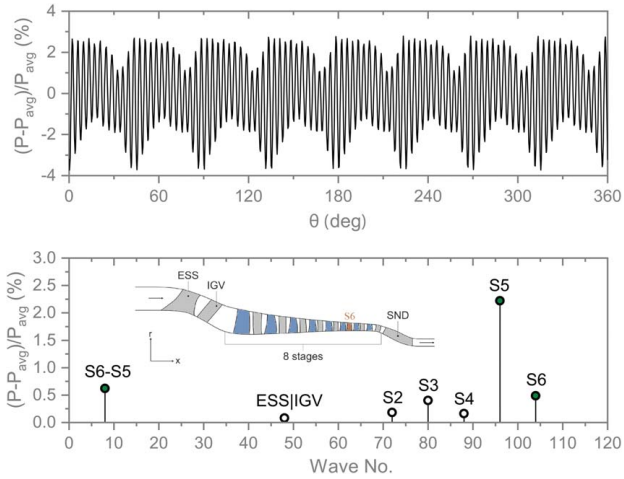

Fig. 1 Circumferential total pressure field at mid-span upstream of stator 6 in a multi-stage axial compressor [10]

To solve an equation of $2N+1$ unknowns, a minimum of the same amount of data points measured at different circumferential locations, $\boldsymbol{\theta} = (\theta_1, \theta_2, \theta_3, \ldots, \theta_m)$, is required. The system can be described with

$$\boldsymbol{AF} = \boldsymbol{x} \tag{4}$$

where $\boldsymbol{A}$ is known as the design matrix with a dimension of $m \times (2N+1)$, $\boldsymbol{F}$ is a vector containing $2N+1$ unknown coefficients, and $\boldsymbol{x}$ is a m-element vector with all the measurement data points from different circumferential locations. The mathematical expressions for $\boldsymbol{A}$, $\boldsymbol{F}$, and $\boldsymbol{x}$ are

$$\boldsymbol{A} = \begin{pmatrix} \sin W_{n,1}\theta_1 & \cos W_{n,1}\theta_1 & \cdots & \sin W_{n,N}\theta_1 & \cos W_{n,N}\theta_1 & 1 \\ \sin W_{n,1}\theta_2 & \cos W_{n,1}\theta_2 & \cdots & \sin W_{n,N}\theta_2 & \cos W_{n,N}\theta_2 & 1 \\ \vdots & \vdots & \vdots & \vdots & \vdots & \vdots \\ \sin W_{n,1}\theta_m & \cos W_{n,1}\theta_m & \cdots & \sin W_{n,N}\theta_m & \cos W_{n,N}\theta_m & 1 \end{pmatrix}$$

$$\boldsymbol{F} = \begin{pmatrix} a_1 \\ b_1 \\ \vdots \\ a_N \\ b_N \\ c_0 \end{pmatrix}$$

$$\boldsymbol{x} = \begin{pmatrix} x(\theta_1) \\ x(\theta_2) \\ \vdots \\ x(\theta_m) \end{pmatrix}$$

To solve for the N wavenumbers of interest described in Eq. (4), the number of data points in vector $\boldsymbol{x}$ must be greater than the number of unknown coefficients or $m \geq 2N+1$. However, in practice, the reconstructed signal contains errors due to the uncertainties in $\boldsymbol{x}(\boldsymbol{\theta})$, and it is critical to evaluate the confidence in the reconstructed signal, which requires additional data points in $\boldsymbol{x}(\boldsymbol{\theta})$. Therefore, a minimum of $2N+2$ measurement points is required to characterize N wavenumbers of interest. However, this yields an over-determined system with more equations than unknowns. In the present study, the method of least-square-fitting is used for solving the unknown coefficients in Eq. (4) for an over-determined system. In Matlab®, this is achieved using the command $\boldsymbol{F} = A\backslash\boldsymbol{x}$ or $\boldsymbol{F} = mldivide(A, \boldsymbol{x})$.

With the magnitude and phase for all the wavenumbers of interest, the circumferential flow field can be reconstructed using Eq. (3). An illustration of reconstruction of the circumferential flow field from spatially under-sampled data using the multi-wavelet approximation method is shown in Fig. 2.

Wavenumbers of Most Importance. Even though the circumferential flow in compressors can be approximated using a few dominant wavelets, resolving all of these wavenumbers can still be challenging. For example, as shown in Fig. 1, the total pressure field in an eight-stage compressor contains seven wavenumbers, which requires a minimum of 15 probes to characterize all of these wavenumbers. However, in practice, due to the cost and blockage associated with each probe, there is usually a limit on the number of probes allowed per blade row. Typically, a range of 3–8 rakes/probes per blade row is achievable and the authors have rarely come across cases of more than 10 rakes/probes for an individual blade row. However, according to Eq. (3), a set of 4, 6, and 8 probes can resolve 1, 2, and 3 wavenumbers, respectively. Thus, an intelligent selection of the most important wavenumbers is critical to assure the best results for reconstructing the signal from a limited number of probes.

The most important wavenumbers can be determined with the help of information from either reduced-order modeling or high-fidelity computational fluid dynamics simulations. For cases with no information available except for airfoil counts, recommended guidelines based on previous research of multi-stage interactions for representative wavenumber selection are

(1) upstream and downstream vane counts;
(2) differences of the upstream and downstream vane counts; and
(3) wavenumbers associated with low-count stationary component (i.e., upstream and downstream struts for the front and rear stages).

Condition Number. The reconstructed flow field using a multi-wavelet approximation method is prone to errors in $\boldsymbol{x}(\boldsymbol{\theta})$ from either uncertainty in probe measurement or in probe positioning. In the linear system described in Eq. (4), the errors in the reconstructed signal are affected by the condition number, k, of the design matrix $\boldsymbol{A}$. The condition number of the design matrix defines the upper bound of the relative errors in $\boldsymbol{F}$ with respect to the relative error in $\boldsymbol{x}$, which is

$$\frac{\|\boldsymbol{\delta F}\|}{\|\boldsymbol{F}\|} \leq k(\boldsymbol{A}) \frac{\|\boldsymbol{\delta x}\|}{\|\boldsymbol{x}\|} \tag{5}$$

The value of the condition number of the design matrix can vary from one to infinity. A system with a large condition number can result in excessive error in the reconstructed signal. There are several formulas for calculation of the condition number of a matrix, and in the present study, the two-norm is used for vector and matrix norm calculation. The condition number is calculated using the formula:

$$k = \|\boldsymbol{A}\| \|\boldsymbol{A}^+\| \tag{6}$$

where $\boldsymbol{A}^+$ is the inverse of matrix $\boldsymbol{A}$ for a square matrix and the Moore–Penrose pseudoinverse of matrix $\boldsymbol{A}$ for a rectangular matrix. In the

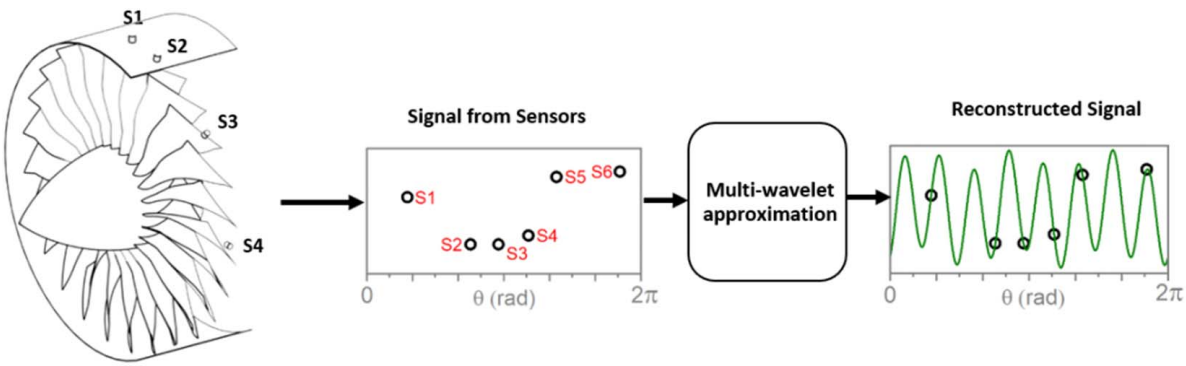

Fig. 2 Sketch of reconstructing the non-uniform circumferential flow using the multi-wavelet approximation method

present study, the condition number of design matrix $\boldsymbol{A}$ is determined by both probe location, $\boldsymbol{\theta}$, and the wavenumbers of interest, $\boldsymbol{W_n}$. Knowing the wavenumbers of interest, the condition number of the design matrix describes how well the probes are distributed to capture the wavenumbers of interest. This is the most important parameter for the selection of probe locations and is, thus, the focus of the following section.

Particle Swarm Optimization. PSO is a well-known optimization technique for solving global optimization problems due to its high efficiency of convergence. It was first introduced by Eberhart and Kennedy [11] for simulation of simplified animal social behaviors such as bird flocking. In the PSO algorithm, a potential solution is called a particle, which has two representative parameters including the position and velocity. The optimization starts with an initial population of particles and then moves these particles around in the search space. The movement of each particle is influenced by its local best-known position as well as the global best-known position in the entire search space. As a result, the swarm is iteratively moving toward the best solution.

In the present study, PSO is used to search for the optimal probe positions that yield the smallest condition number of the design matrix. The same algorithm was used to optimize the probe positions for blade tip timing with success [12]. The design variables (parameters being optimized) are the circumferential position of probes, $\boldsymbol{\theta}$, and the objective function is described using:

$$f_{\text{obj}} = k(\boldsymbol{\theta}, \boldsymbol{W_n}) + f_{\text{constraint}} \tag{7}$$

where $f_{\text{constraint}}$ represents the value of the constraint function from considerations of geometric constraints for placing probes. Two representative constraints in turbomachines include minimum spacing between adjacent probes and restricted areas due to casing fixtures. Probes in turbomachines are typically casing-mounted through a variety of instrumentation ports. A minimum probe spacing is, therefore, necessary for practical implementation. The formula for minimum probe spacing is described as

$$|\Delta\theta_{j,i}| = |\theta_j - \theta_i| \geq \theta_{\min} \tag{8}$$

Additionally, in many scenarios, it may not be possible to install probes at all positions around the circumference due to fixtures or obstructions on certain regions of the casing. A constraint is, therefore, required to prevent probes from being placed in these circumferential ranges. The formula for constraints due to casing fixtures is described as

$$\theta_i \tilde{\in} [\theta^*_{1,\min}, \theta^*_{1,\max}] | [\theta^*_{2,\min}, \theta^*_{2,\max}] \ldots | [\theta^*_{p,\min}, \theta^*_{p,\max}] \tag{9}$$

in which, $\theta^*_{p,\min}$ and $\theta^*_{p,\max}$ represent the minimum and maximum fixture location for the pth fixture. During the optimization process, if the position of any probe violates any of the constraints, a "penalty" or "cost" will be assigned to the constraint function to prevent probe placement in that region. At last, it is worth noting that the PSO used in the present study can also be exchanged by other global optimization techniques for probe optimization.

Confidence in Reconstructed Signal. It is important to gauge the confidence in the reconstructed circumferential flow obtained from the multi-wavelet approximation method. To achieve this objective, two parameters, including the Pearson correlation coefficient and root-mean-square of the fitting residual, are proposed.

The Pearson correlation coefficient, or Pearson's r, is a measure of the linear correlation between two variables. Its magnitude varies between 0 and 1, with values close to 1 indicating a strong linear correlation. In the present study, the two variables used for correlation are the predicted flow properties, $\boldsymbol{x}_{\text{fit}}(\boldsymbol{\theta})$, from the reconstructed signal and the true measurements, $\boldsymbol{x}(\boldsymbol{\theta})$. The formula for calculating the Pearson correlation coefficient i

$$\rho = \frac{\sum_{j=1}^{m} x_j x_{\text{fit},j} - \left(\sum_{j=1}^{m} x_j \sum_{j=1}^{m} x_{\text{fit},j}\right)/m}{\sqrt{\left(\sum_{j=1}^{m} x_j^2 - \left(\sum_{j=1}^{m} x_j\right)^2/m\right)\left(\sum_{j=1}^{m} x_{\text{fit},j}^2 - \left(\sum_{j=1}^{m} x_{\text{fit},j}\right)^2/m\right)}} \tag{10}$$

For a well-reconstructed circumferential flow field, the predicted flow properties will align with true values at all the measurement locations and yield a value of nearly 1 for the Pearson's r. In contrast, the predicted flow properties from a poorly reconstructed flow field will deviate from the true measurements resulting in a small value for Pearson's r.

In addition to Pearson's r, the confidence in the reconstructed flow can also be evaluated in terms of the root-mean-square of the fitting residual between the reconstructed signal and true measurements. The formula for calculating R_{rms} is

$$R_{\text{rms}} = \sqrt{\frac{1}{m}\left(\sum_{j=1}^{m} (x_{\text{fit},j} - x_j)^2\right)} \tag{11}$$

Proof-of-Concept

The objectives for the proof-of-concept include

(1) Examine the effectiveness of the PSO method for probe position optimization.
(2) Examine the effectiveness of the multi-wavelet approximation method in resolving the magnitude and phase information of the wavenumbers of interest.
(3) Examine the effectiveness of the multi-wavelet approximation method in reconstructing the true circumferential flow field.

The case selected for proof-of-concept is the total pressure field at mid-span upstream of stator 6 in an eight-stage axial compressor representative of an aero-engine small core compressor available in the open literature [10], as shown in Fig. 1. Information of the total pressure field are obtained from a full-annulus URANS simulation and are referred as the "true flow field" in the rest of the paper. The selected total pressure field includes seven dominant wavelets due to the complex blade row interactions in a multi-stage environment and, therefore, provides an ideal case for the proof-of-concept and method validation purposes.

Probe Position Optimization Using Particle Swarm Optimization. With the information of upstream and downstream stator row vane counts, the three wavenumbers of highest interest are those associated with the vane counts for *S*5, *S*6, and the difference in the counts, *S*6–*S*5, following the guidelines provided in the previous section. The wavenumber for the *S*5 count captures the effect of the wakes from stator 5, the wavenumber of the *S*6 count captures the effect of the potential field of stator 6, and the wavenumber of the difference in vane counts (*S*6–*S*5) will capture the interaction of stators 5 and 6. As a result, a minimum of seven probes are required to resolve these three wavenumbers. In the present case, the number of probes for signal reconstruction is selected to be 8, which allows one extra data point for evaluation of the confidence in the reconstructed flow.

The goal of probe position optimization is to characterize the combination of the three wavenumbers of interest, as well as all possible subsets of wavenumber combinations. The optimal probe set is defined as the probe position leading to the minimum sum of the squared weighted condition numbers of all the wavenumber combinations. In the present study, three wavenumbers of interest yield a total of seven wavenumber combinations. The objective function is

expressed as

$$f_{\text{obj}} = \sum_{i=1}^{7} [a_{W_n} k(\boldsymbol{\theta}, \boldsymbol{W_n})]^2 + f_{\text{constraint}} \tag{12}$$

where a_{W_n} represents the weighting factor for a combination of wavenumbers $\boldsymbol{W_n}$. In the present study, no specific emphasis was placed on certain wavenumber combinations, and the same weighting factor was used for all of the wavenumber combinations. For all optimization runs conducted in this paper, a particle swarm size of 5000 was chosen, and the optimization was run for 100 iterations. Figure 3 shows the change in the value of objective function during one optimization run. Results show that the value of the objective function decreases quickly during the first 20 iterations and gradually settles around 19 after 60 iterations. Therefore, a selection of 100 iterations is a proper number for the present case study.

The final probe positions from the run shown in Fig. 3 are indicated by the red circle in Fig. 4(*a*). One evident feature associated with the optimized probe set is that they are not equally spaced. The maximum probe spacing falls between P3 and P4, with a value of 62 deg, while the minimum probe spacing is 20 deg. This non-uniform probe spacing allows for characterization of all wavenumbers of interest. As shown in Fig. 4(*b*), the condition numbers are fairly constant for all combinations of wavenumbers. This is expected and also consistent with the nature of the objective function, which had a constant weighting factor for all combinations of wavenumbers. The largest condition number for all the combinations of wavenumbers is less than 2. This indicates that the optimized probe set can discern all the wavenumbers of interest. In summary, it has been demonstrated that the PSO algorithm is capable of optimizing probe positions effectively, yielding small condition numbers for all wavenumbers of interest.

Figure 5 shows the values of Pearson's r (top) and the root-mean-square of the fitting residual (bottom) for all wave number combinations. The predicted optimal wavenumber combinations for single-, double-, and triple-wavelet approximations are indicated by the second, fourth, and last columns in the chart. For the single-wavelet approximation, the predicted dominant wave number, in terms of highest Pearson's r and smallest fitting residual, equates to the vane count of stator 5 (*S*5, vane count 96). For the double-wavelet approximation, the predicted dominant wavenumbers are *S*5 and *S*6–*S*5. Comparing to the single-wavelet approximation using wavenumber of *S*5, inclusion of the second wavenumber *S*6–*S*5 yields higher confidence in the reconstructed signal (higher value of Pearson's r and smaller residual error). At last, a

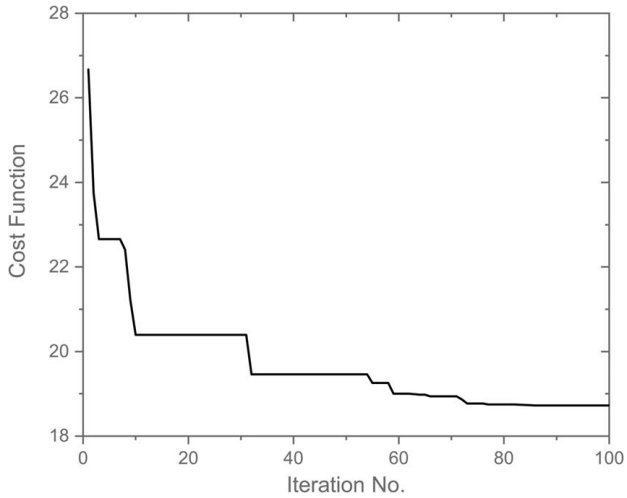

Fig. 3 Illustration of the changes in the objective function during the optimization of a probe set using PSO

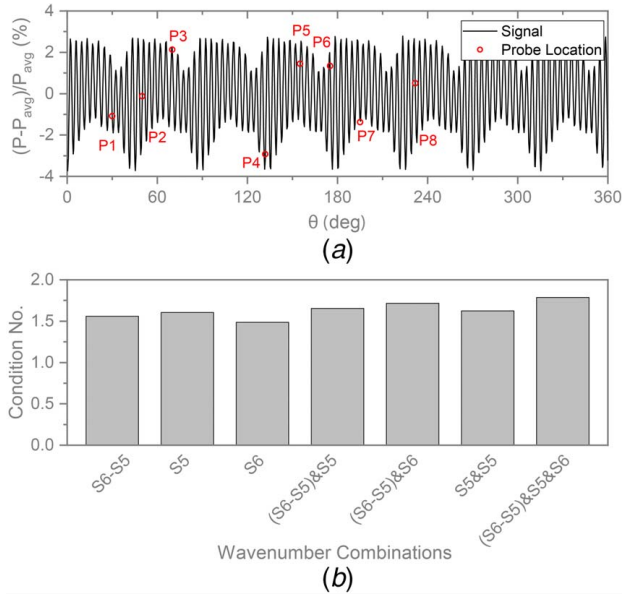

Fig. 4 (*a*) Optimized probe positions and (*b*) condition number for all combinations of possible wave numbers

wavenumber set of *S*5, *S*6–*S*5, and *S*6 (vane count 104) yields the highest fitting confidence and smallest fitting residual among all the seven wavenumber combinations.

Table 1 lists the values of Pearson's r and fitting residual, as well as the rank of individual wavenumber combination. The rank for the three wavenumbers of interest agrees with the results from the spatial wavenumber analysis of the true signal shown in Fig. 1. In other words, the importance of all the wavenumbers of interest can be quantified and correctly ranked using two parameters: the Pearson correlation coefficient and the fitting residual. Finally, the trend in the value of the Pearson correlation and fitting residual from single- to multi-wavelet approximation can gauge the necessity of including additional wavenumbers. For example, in the present case, the fitting confidence in terms of Pearson's correlation is 99.9% with a fitting residual of less than 0.1% after including three wavenumbers and, thus, indicates little need to include additional wavenumbers.

Furthermore, details of true data and fitting data at all measurement locations from the best cases using single-, double-, and

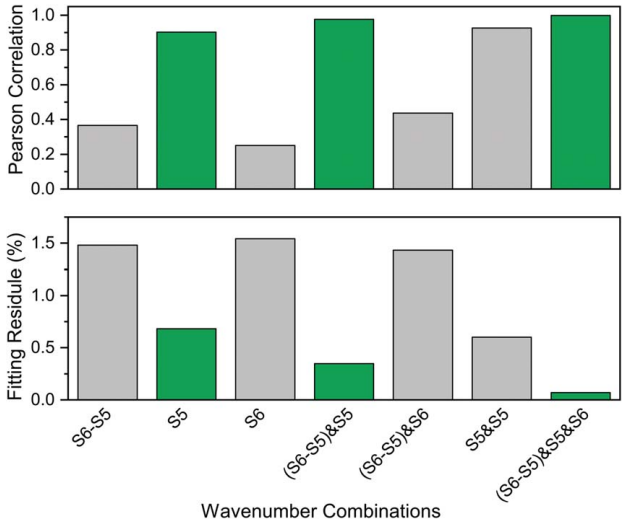

Fig. 5 Values of Pearson's r (top) and fitting residual (bottom) for all possible wave number combinations

Table 1 Rank of data fitting for a variety of wavenumber combinations

Wave no. combination	Pearson correlation	Fitting residual	Rank
8 (S6–S5)	0.366	1.482	5
96 (S5)	0.903	0.683	4
104 (S6)	0.251	1.541	7
[8, 96]	0.976	0.347	2
[8, 104]	0.437	1.433	6
[96, 104]	0.926	0.601	3
[8, 96, 104]	0.999	0.070	1

triple-wavelet approximation are shown in Fig. 6. Figure 6(*a*) shows both the data from the true measurements and the reconstruction using the multi-wavelet approximation. Figure 6(*b*) shows the deviation between these two data sets. There is significant improvement in data fitting with the additional wavelets. For example, the best case from the single-wavelet approximation still has large deviations between the fitting and true data at almost all measurement locations (except for P2), resulting in a maximum of four points in variation between the fitting data and true measurements, as indicated by the shaded band in Fig. 6(*b*). The data from double-wavelet approximation show significant improvement in matching the true measurements. Furthermore, the fitting using the three-wavelet approximation shows good agreement with the true measurements at all the probe locations. The variation between the fitting data and true measurements is ten times smaller (< 0.3 points) compared to the results from single-wavelet approximation.

Comparison of the reconstructed total pressure field from the best cases of single-, double-, and triple- approximation with the true total pressure field is shown in Fig. 7. Figure 7(*a*) shows the comparison in the spatial domain while Fig. 7(*b*) shows the comparison in magnitudes at specific wavenumbers. There is significant difference in the reconstructed signal using single-wavelet approximation from the true signal, and this is due to the absence of low wavenumber (*S6–S5*) components. The deviation between the reconstructed and true signal is much reduced in the results using the double-wavelet approximation. Finally, the reconstructed circumferential total pressure obtained from a triple-wavelet approximation shows very good agreement with the true total pressure field.

Additionally, the predicted magnitude at specific wavenumbers from the single-, double-, and triple-approximation methods show fairly good agreement with the true signal, as shown in Fig. 7(*b*). The largest error occurs at the low wavenumber (*S6–S5*) with a 32.5% over-prediction in magnitude. The errors in the predicted magnitudes at the two large wavenumbers, *S5* and *S6*, are within 5%, as shown in Table 2. There is less error in the predicted phase magnitude, with a maximum error of less than 10% at wavenumber *S6*.

To summarize, the circumferential total pressure field in a multistage compressor representative of small core compressors is reconstructed using a few spatially under-sampled data points. To start with, the three wavenumbers of most importance were selected following the guidelines presented in the previous section. This also led to a selection of eight probes to reconstruct the circumferential flow. Following that, the circumferential locations of the eight probes were carefully selected using the PSO algorithm. The PSO algorithm can optimize probe positions leading to small condition numbers for all the wavenumber of interest. Finally, the circumferential total pressure is reconstructed from the eight data points using a triple-wavelet approximation and very good agreement between the reconstructed signal and the true signal was achieved.

Sensitivity Analysis

As discussed in the previous section, the reconstructed flow field using the multi-wavelet approximation method is prone to errors. There are two sources of error. The first is the systematic error associated with the multi-wavelet approximation method since a limited number of wavelets are utilized. The second is due to the error propagation from the uncertainties in probe measurement and position. To reduce the systematic error, an increase in the number of probes is required to allow for characterization of more wavenumbers. As to the error propagation from measurement uncertainties and tolerances in probe positions, a probe set yielding a smaller condition number tends to introduce less error to the reconstructed flow. It was shown in the previous section that a set of eight probes is sufficient to reconstruct the circumferential flow in an aero-engine small core compressor with high accuracy. However, no guidelines have been drawn on the range for the condition number of the design matrix. Additionally, because of the random nature of the PSO algorithm and the multitude of local minima, the optimized probe positions can vary from run to run. Thus, it is important to understand the influence of the variations in optimized probe positions on the errors in the reconstructed flow. To bridge this gap, the

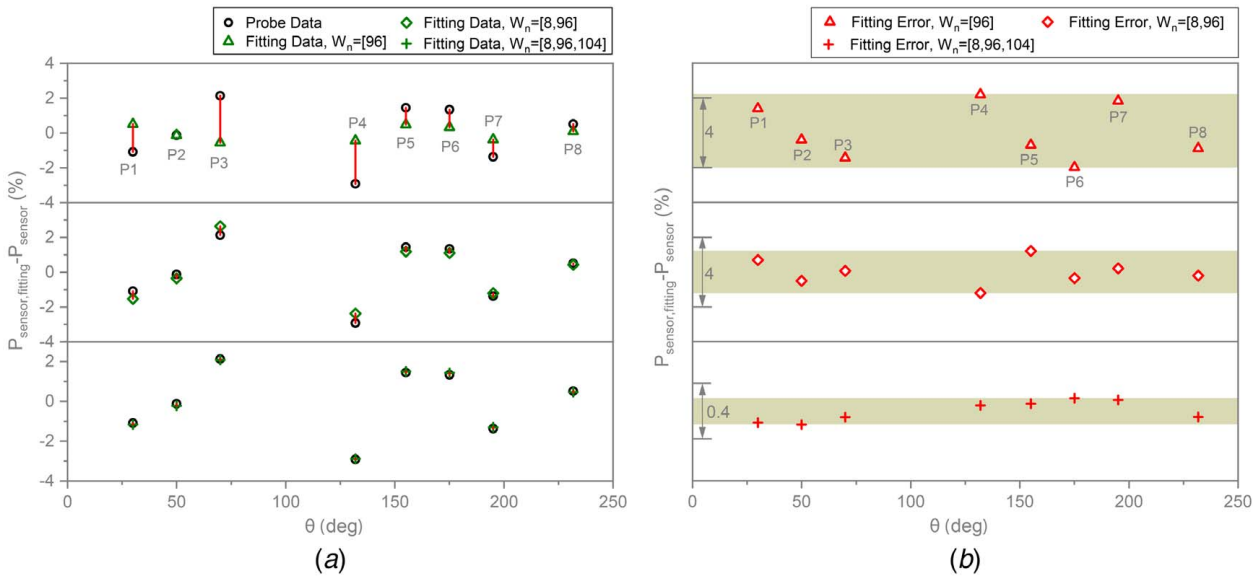

Fig. 6 Comparison of the (*a*) true measurement and fitting data and (*b*) associated fitting errors from the best cases using single-, double-, and triple-wavelet approximation

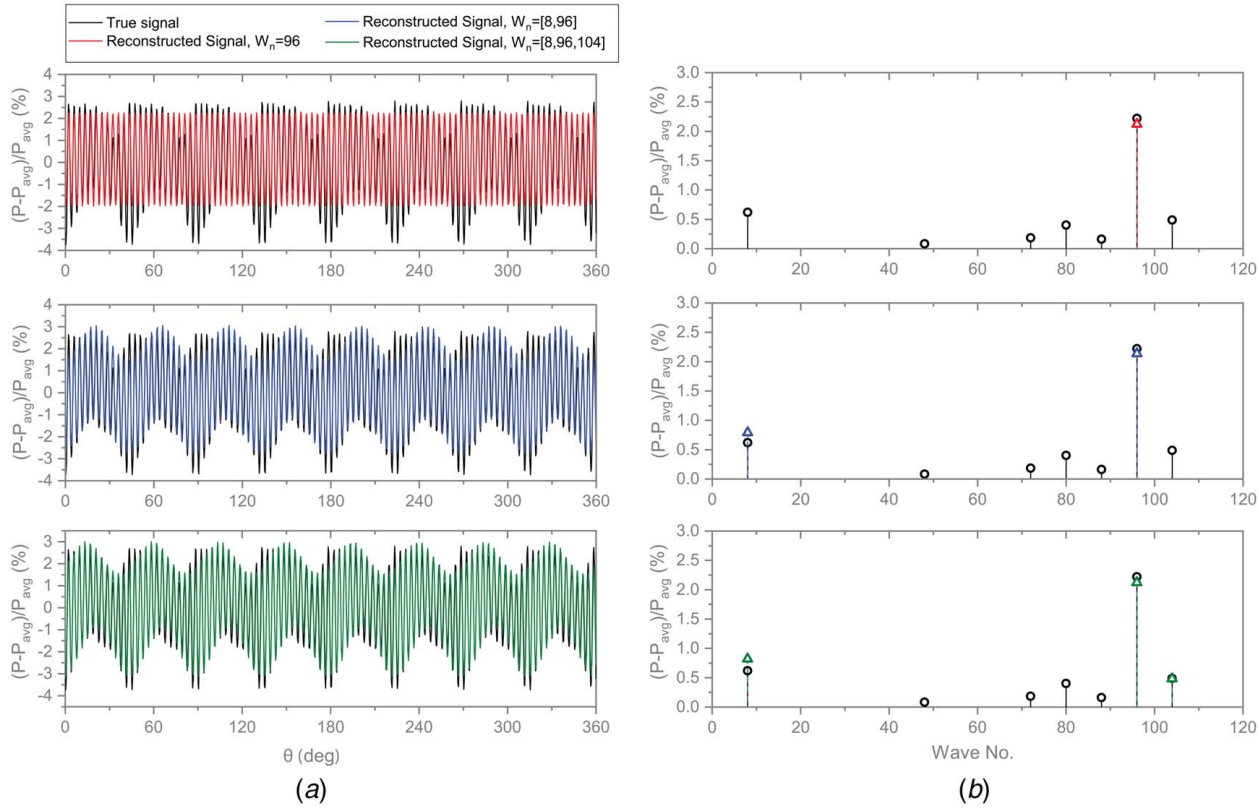

Fig. 7 Comparison of true and reconstructed total pressure field in (*a*) spatial and (*b*) frequency domain from single-, double-, and triple-wavelet approximation

influence of the design matrix condition number and the influence of the random nature of the optimized probe positions on the error in the reconstructed signal were investigated.

Influence of Condition Number. The discussions in the present section are organized in the following manner. First, the role of the condition numbers of the design matrix in error propagation is illustrated by comparing the reconstructed signals obtained from a good probe configuration with those from a poor probe configuration. Following that, the effects of condition number on the errors in the reconstructed signal are quantified and guidelines for the upper limit of the condition number of the design matrix are drawn. To be consistent with results in the previous section, the same circumferential total pressure field, shown in Fig. 1, was used for all the analyses presented in this section.

The positions for the good and poor probe configurations are shown in Fig. 8. Both configurations have a total of eight probes and the position of the first probe is the same for both sets. As listed in Table 3, the difference in the two probe sets is the spacing between the probes. The good probe configuration is the probe set optimized using PSO, as shown in Fig. 3. The probes are spaced in a non-uniform manner to resolve all three wavenumbers of interest. The probes in the poor configuration are equally spaced, at 18 deg intervals. The condition number of the good probe set for the combination of wavenumbers $\boldsymbol{W_n} = [S6–S5, S5, S6]$ is 1.78. In contrast, the condition number of the poor probe set is on the magnitude of 10^{14}. The errors in the measurements from each probe are indicated by the error bars in Fig. 8. The abscissa error bar represents the geometric tolerance for probe installation while the ordinate error bar represents the uncertainty in the measurement of each sensor. For the analysis presented in this section, a ±0.1 deg uncertainty in probe circumferential position and ±0.25% accuracy full scale for the pressure sensors are selected.

Figure 9 shows the histogram of errors in the reconstructed signal from 10,000 sets of data points. Each data set, $\boldsymbol{x}_{\text{noise}}$, was generated by adding a random error in probe measurement and random error associated with tolerances in probe position and described as

$$\boldsymbol{x}_{\text{noise}} = \boldsymbol{x} + rand(\boldsymbol{e_m}) + rand(\boldsymbol{e_p}) \tag{13}$$

where $\boldsymbol{e_m}$ is the probe measurement error and $\boldsymbol{e_p}$ is the error associated with probe positioning tolerance. The results from the good probe configuration are shown in Fig. 9(*a*), and the results from

Table 2 Comparison of magnitude and phase at wavenumbers of interest from multi-wavelet approximation with true signal

	Magnitude (%)			Phase (rad)		
Wave no.	True	Fitting	Error	True	Fitting	Error
8 (S6–S5)	0.62	0.83	32.5	5.42	5.23	3.6
96 (S5)	2.22	2.12	4.4	4.19	4.13	1.4
104 (S6)	0.49	0.49	0.8	3.96	3.61	8.9

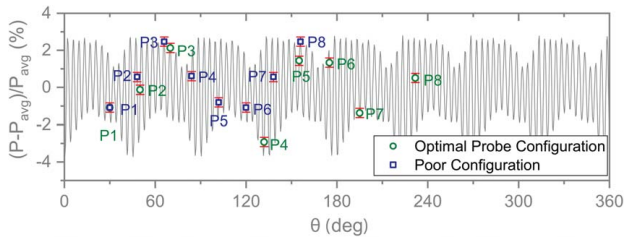

Fig. 8 The positions of a good and poor probe set

Table 3 The positions and condition number for the good and poor probe set

Config.	Circumferential positions	Condition no.
Good	[30 deg, 50 deg, 70 deg, 132.0 deg, 155.1 deg, 175.1 deg, 195.1 deg, 231.8 deg]	1.79
Poor	[30 deg, 48 deg, 66 deg, 84 deg, 102 deg, 120 deg, 138 deg, 156 deg]	3.67×10^{14}

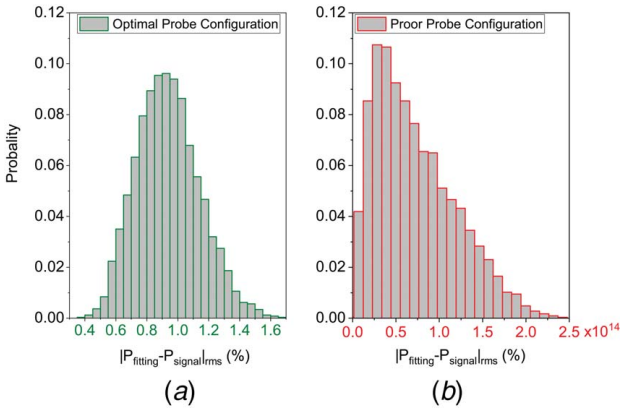

Fig. 9 Representative of well-conditioned and ill-conditioned probe configurations

the poor probe configuration are shown in Fig. 9(*b*). The error in the reconstructed total pressure field using the good probe set varies from 0.4% to 1.6%, with the majority of the values around 1.0%. In contrast, the errors in the reconstructed signal using the poor probe set is extremely large on the order of 10^{14}.

Figure 10 shows the reconstructed signal using the error-free input data, as well as the best- and worst-reconstructed signals. The results from the good probe set are shown in Fig. 10(*a*), and the results from the poor probe set are shown in Fig. 10(*b*). The reconstructed circumferential total pressure field using the good probe set shows good agreement with the true flow in all three cases, even for the worst scenario using input data with errors. However, for the poor probe configuration, there is significant error in the reconstructed signal, even when using the error-free input data. Furthermore, the poor probe set failed to reconstruct the total pressure field using the input data with error. The errors in the reconstructed signal for the best scenario are extremely large on the order of 10^{11}. To conclude, the condition number of the design matrix plays a critical role in the quality of the reconstructed circumferential flow. The smaller the condition number, the less error it introduces to the reconstructed flow. A probe set of large condition number can yield excessive errors in the reconstructed signal.

Additionally, the effect of the condition number of the design matrix on the errors in the reconstructed signal is quantified. A total of ten sets of probes are selected, and the corresponding condition number of the design matrix for these probe sets varies from 2 to 20. At each condition number, the error range of the reconstructed signal from 10,000 sets of data points with randomly generated errors is shown in Fig. 11. As expected, there is a general trend of increased error in the reconstructed signal as the condition number increases. However, a probe set with a large condition number can yield a well-reconstructed signal of small error, but the smaller condition number does give a smaller error band, or high confidence interval, in the reconstructed signal. Based on the trend shown in Fig. 11, it is recommended to use a probe set of condition number less than 4 to assure best results in the reconstructed signal.

Influence of Probe Configurations. Due to the random nature of the PSO algorithm and the multitude of local minima, the

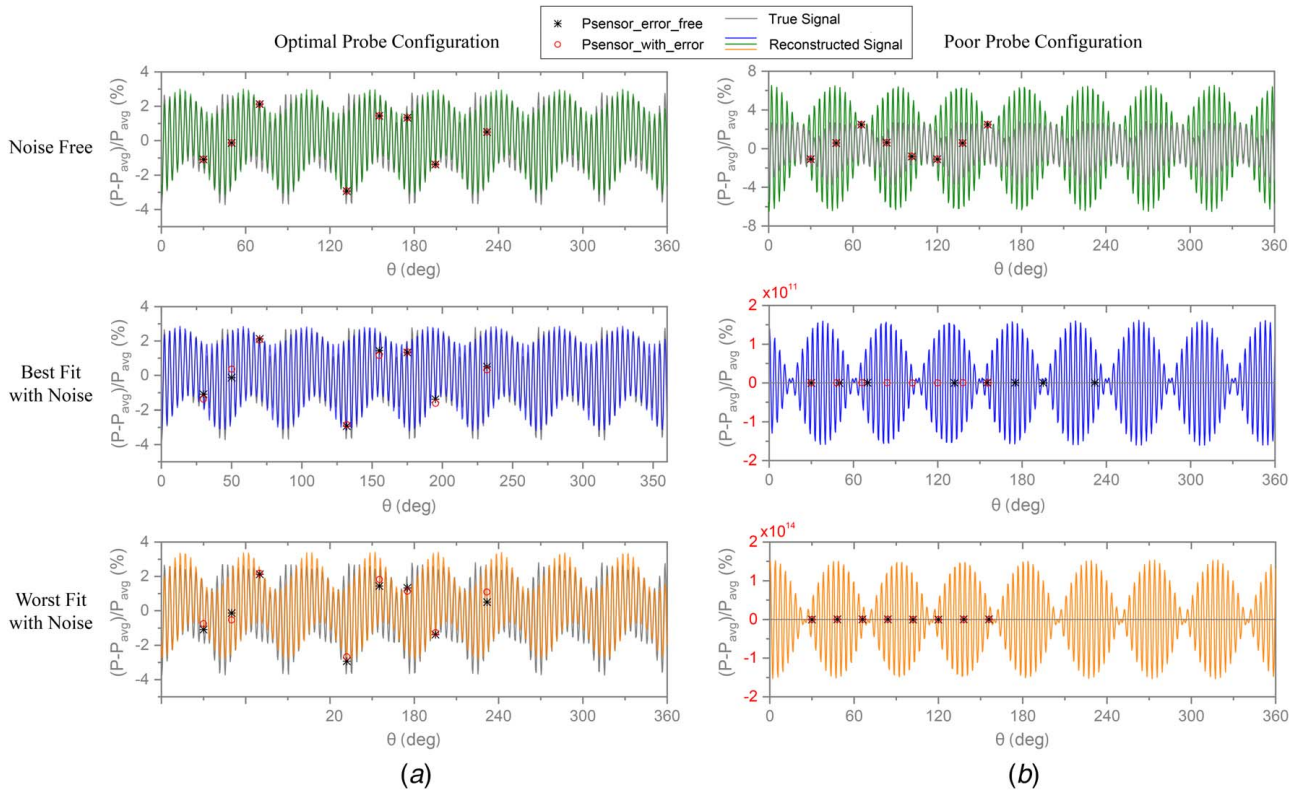

Fig. 10 Comparison of reconstructed signal with true signal from (*a*) a good probe set and (*b*) a poor probe set

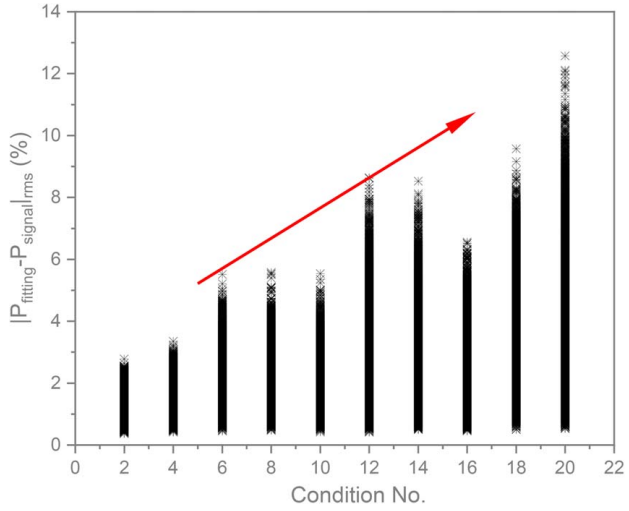

Fig. 11 Effect of design matrix's condition number on the errors in the reconstructed signal

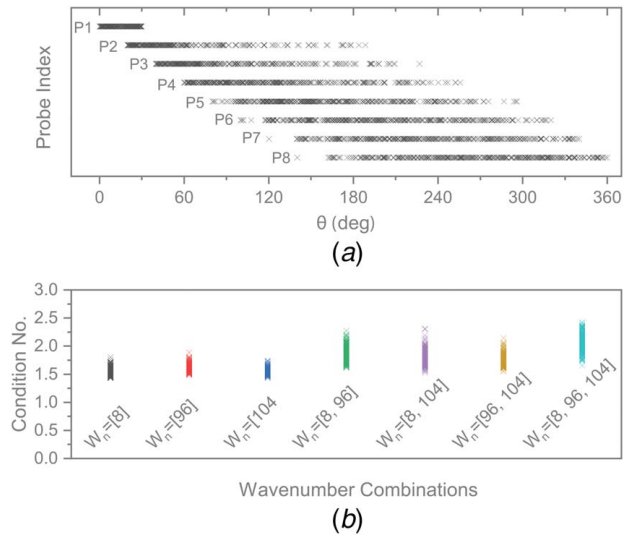

Fig. 12 (*a*) Optimized probe positions from 500 runs and (*b*) the values of their design matrix's condition number

optimized probe positions can vary from run to run. Figure 12(*a*) shows the results of the optimized probe positions from 500 runs. The position of each probe is indicated by a cross. The optimized probe positions are distributed over a broad range of the circumference. However, the condition number for all the optimized probe sets is of similar magnitude, as shown in Fig. 12(*b*). The maximum value of the design matrix is less than 2.5. To understand the influence of the variations in optimized probe positions on the quality of the reconstructed signal, the root-mean-square error in the reconstructed signal from the 500 different probe sets is shown in Fig. 13(*a*). The abscissa is the averaged probe spacing of the optimized probe set, and the ordinate represents the root-mean-square error of the reconstructed signal. The errors in the reconstructed signal from 500 different probe sets are very small, less than 0.24%. This shows that, regardless of the variations in the optimized probe positions from run to run using PSO, they all yield a well-reconstructed circumferential flow. Additionally, Fig. 13(*b*) shows the errors in the reconstructed signal from a variety of equally spaced probe sets. For comparison, the error bands from the optimized probes are highlighted. There is about a 20:1 variation in the errors of the reconstructed signal depending

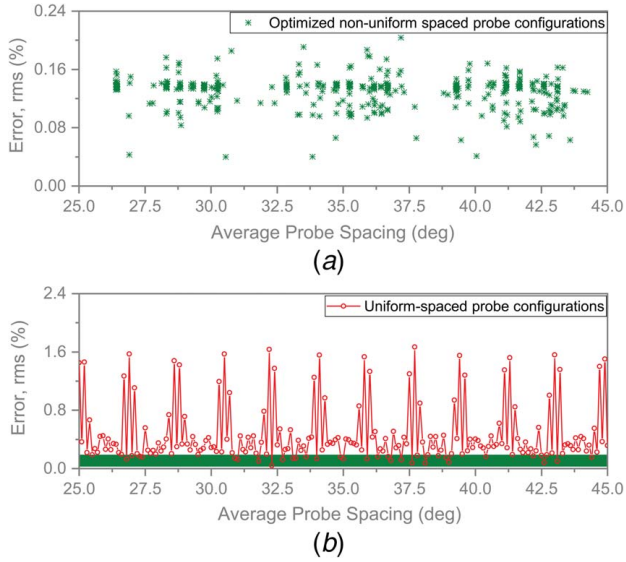

Fig. 13 Errors in the reconstructed signal from (*a*) optimized probe sets and (*b*) equally spaced probe sets

on the value of probe spacing. Although there are occasional cases where equally spaced probe sets yield similar magnitude, or even smaller error, in the reconstructed signal, the equally spaced probe set typically yields much larger errors in the reconstructed signal. Thus, one important takeaway from the sensitivity analysis can be drawn: if circumstance allows, the location of the probes shall be optimized to yield best results for flow reconstruction. Otherwise, there can be significant error introduced to the reconstructed signal due to the large condition number associated with the probe set, particular for an equally spaced probe set.

Conclusions

The flow field in a compressor is circumferentially non-uniform due to the wakes from upstream stators as well as the potential field of adjacent stationary rows. Characterization of this non-uniform flow is of great importance since it can affect stage performance and blade forced response. Historically, experimental characterization of the circumferential flow variation is achieved by circumferentially traversing either a probe or the stator rows, which requires complex and costly traverse mechanisms. To address this challenge, this paper presents a novel method to reconstruct the circumferentially non-uniform flow in turbomachines using spatially under-sampled data points from a few probes instrumented at fixed circumferential locations. The method includes two core techniques:

(1) PSO algorithm for selection of optimal probe position.
(2) Multi-wavelet approximation method to reconstruct the non-uniform circumferential flow from several dominant wavenumbers.

The roadmap for implementation of the method includes:

(1) Identify the most important wavenumbers and determine the number of probes.
(2) Select the optimal probe positions using the PSO algorithm.
(3) Reconstruct the circumferential flow using the multi-wavelet approximation.
(4) Evaluate the confidence in the reconstructed signal in terms of Pearson's r and root-mean-square of fitting residual.

Validation of the method is performed using the total pressure at mid-span upstream of stator 6 in an eight-stage axial compressor representative of an aero-engine small core compressor. The

circumferential variations in the total pressure field are dominated by seven wavenumbers associated with the vane counts of the blade rows upstream and downstream of stator 6 and, therefore, provides an ideal case for proof-of-concept and method validation. Following that, a sensitivity analysis of the method is conducted to study the influence of probe spacing on the error in the reconstructed signal. A summary of the results includes:

(1) The three most important wavenumbers were selected following the guidelines provided in the methodology section, which also led to the selection of eight probes to reconstruct the circumferential flow.
(2) The PSO algorithms determined the optimized probe positions that lead to small condition numbers for all the wavenumbers of interest.
(3) The multi-wavelet approximation method resolved both the magnitude and phase of the wavenumbers of interest with relatively good accuracy.
(4) The circumferential total pressure field is reconstructed from eight data points using a triple-wavelet approximation, and very good agreement between the reconstructed signal and the true signal was achieved.
(5) A design matrix with a larger condition number leads to a greater chance of introducing larger errors into the reconstructed signal.
(6) A condition number smaller than 4 is recommended to assure optimal results in the reconstructed signal.
(7) The optimal probe positions can vary from run to run due to the random nature of the PSO algorithm, but the influence of this random nature in the optimized probe position on the errors in the reconstructed signal is negligible.

To conclude, a roadmap for reconstructing the non-uniform circumferential flow in turbomachines using spatially under-sampled data points was established. The method was shown to be robust and capable of reconstructing the compressor circumferential flow field with good accuracy. Furthermore, in the second part of this paper, this method is applied to two compressor component-level experiments to further demonstrate the potential of this novel method in resolving the important flow features associated with circumferential flow non-uniformity.

Conflict of Interest

There are no conflicts of interest.

Data Availability Statement

The datasets generated and supporting the findings of this article are obtained from the corresponding author upon reasonable request.

References

[1] He, L., Chen, T., Wells, R. G., Li, Y. S., and Ning, W., 2002, "Analysis of Rotor–Rotor and Stator–Stator Interferences in Multi-Stage Turbomachines," ASME J. Turbomach., **124**(4), pp. 564–571.
[2] Key, N. L., Lawless, P. B., and Fleeter, S., 2010, "An Experimental Study of Vane Clocking Effects on Embedded Stage Performance," ASME J. Turbomach., **132**(1), p. 011018.
[3] Choi, Y. S., Key, N., and Fleeter, S., 2011, "Vane Clocking Effects on the Resonant Response of an Embedded Rotor," J. Propul. Power, **27**(1), pp. 71–77.
[4] Salontay, J. R., Key, N. L., and Fulayter, R. D., 2011, "Investigation of Flow Physics of Vane Clocking Effects on Rotor Resonant Response," J. Propul. Power, **27**(5), pp. 1001–1007.
[5] Terstegen, M., Sanders, C., Jeschke, P., and Schoenenborn, H., 2019, "Rotor–Stator Interactions in a 2.5-Stage Axial Compressor—Part I: Experimental Analysis of Tyler–Sofrin Modes," ASME J. Turbomach., **141**(10), p. 101002.
[6] Sanders, C., Terstegen, M., Jeschke, P., Schönenborn, H., and Heners, J. P., 2019, "Rotor–Stator Interactions in a 2.5-Stage Axial Compressor, Part II: Impact of Aerodynamic Modelling on Forced Response," ASME J. Turbomach., **141**(10), p. 101008.
[7] Stoll, F., Tremback, J. W., and Arnaiz, H. H., 1979, "Effect of Number of Probes and Their Orientation on the Calculation of Several Compressor Face Distortion Descriptors," Technical Report, NASA Technical Memorandum 72859.
[8] Cumpsty, N. A., and Horlock, J. H., 2006, "Averaging Nonuniform flow for a Purpose," ASME J. Turbomach., **128**(1), pp. 120–129.
[9] Stummann, S., Jeschke, P., and Metzler, T., 2015, "Circumferentially Non-Uniform Flow in the Rear Stage of a Multistage Compressor," ASME Turbo Expo 2015: Turbine Technical Conference and Exposition, Montreal, Canada, June 15–19, American Society of Mechanical Engineers Digital Collection.
[10] Chilla, M., Pullan, G., and Gallimore, S., 2019, "Reducing Instrumentation Errors Caused by Circumferential Flow Field Variation in Multi-Stage Axial Compressors," ASME Turbo Expo 2019: Turbomachinery Technical Conference and Exposition, American Society of Mechanical Engineers, Phoenix, AZ, June 17–21, pp. 1–11.
[11] Eberhart, R., and Kennedy, J., 1995, "A New Optimizer Using Particle Swarm Theory," Proceedings of the Sixth International Symposium on Micro Machine and Human Science, Nagoya, Japan, Oct. 4–6.
[12] Diamond, D. H., and Stephan Heyns, P., 2018, "A Novel Method for the Design of Proximity Sensor Configuration for Rotor Blade Tip Timing," ASME J. Vib. Acoust., **140**(6), p. 061003.